Acta Pharmacologica Sinica

www.nature.com/aps

ARTICLE

Discovery and characterization of a novel cGAS covalent inhibitor for the treatment of inflammatory bowel disease

Jia Song[1,2], Rui-rui Yang[2,3,4], Jie Chang[2], Ya-dan Liu[5], Cheng-hao Lu[5], Li-fan Chen[2,3], Hao Guo[2,3], Ying-hui Zhang[2,3], Zi-sheng Fan[2,5], Jing-yi Zhou[2,5], Gui-zhen Zhou[2,5], Ke-ke Zhang[2,5], Xiao-min Luo[2,3,5], Kai-xian Chen[2,3,5], Hua-liang Jiang[1,2,3,4,5], Su-lin Zhang[2,3] and Ming-yue Zheng[2,3,5]

Cyclic GMP-AMP synthase (cGAS), a cytosolic DNA sensor, acts as a nucleotidyl transferase that catalyzes ATP and GTP to form cyclic GMP-AMP (cGAMP) and plays a critical role in innate immunity. Hyperactivation of cGAS-STING signaling contributes to hyperinflammatory responses. Therefore, cGAS is considered a promising target for the treatment of inflammatory diseases. Herein, we report the discovery and identification of several novel types of cGAS inhibitors by pyrophosphatase (PP_iase)-coupled activity assays. Among these inhibitors, 1-(1-phenyl-3,4-dihydro-1*H*-pyrrolo[1,2-a]pyrazin-2-yl)prop-2-yn-1-one (compound **3**) displayed the highest potency and selectivity at the cellular level. Compound **3** exhibited better inhibitory activity and pathway selectivity than RU.521, which is a selective cGAS inhibitor with anti-inflammatory effects in vitro and in vivo. Thermostability analysis, nuclear magnetic resonance and isothermal titration calorimetry assays confirmed that compound **3** directly binds to the cGAS protein. Mass spectrometry and mutation analysis revealed that compound **3** covalently binds to Cys419 of cGAS. Notably, compound **3** demonstrated promising therapeutic efficacy in a dextran sulfate sodium (DSS)-induced mouse colitis model. These results collectively suggest that compound **3** will be useful for understanding the biological function of cGAS and has the potential to be further developed for inflammatory disease therapies.

Keywords: cyclic GMP-AMP synthase; covalent inhibitor; inflammatory bowel disease; high-throughput screening

Acta Pharmacologica Sinica (2023) 44:791–800; https://doi.org/10.1038/s41401-022-01002-5

INTRODUCTION

The innate immune system, which is a natural line of defense, recognizes pathogen invasion using pattern-recognition receptors (PRRs) [1], which include cytoplasmic DNA sensors and cGAS [2]. Growing evidence indicates the essential role of cGAS in innate immunity, and its role mainly depends on the cGAS-STING signaling pathway. As shown in Fig. 1, cGAS can recognize and interact with pathogenic double-stranded DNA (dsDNA), which induces conformational changes in the active site of cGAS [3], thereby catalyzing the synthesis of cGAMP from adenosine triphosphate (ATP) and guanosine triphosphate (GTP) [4, 5]. Then, as a second messenger, cGAMP can bind to the downstream signaling molecule stimulator of interferon genes (STING) and induce its conformational change to become an active polymer [6–8]. Activated STING translocates from the endoplasmic reticulum to perinuclear vesicles and recruits and activates TANK binding kinase 1 (TBK1) and IκB kinase (IKK) to induce the expression of type I interferons (IFNs) and proinflammatory cytokines [9–11].

Notably, cGAS has no nucleotide sequence specificity for DNA recognition [12], which means that it can also be activated by self-DNA. The hyperactivation of cGAS-STING signaling caused by self-DNA due to nuclear leakage or mitochondrial damage is likely to cause autoimmune and inflammatory diseases [13, 14]. For example, deficiency or mutation in the *Trex1* gene, which encodes the mammalian 3′-5′DNA exonuclease, causes cytoplasmic DNA accumulation and subsequent activation of the cGAS-STING signaling pathway, which is responsible for Aicardi-Goutières syndrome (AGS) and systemic lupus erythematosus (SLE) [15–17]. Depletion of cGAS can rescue autoimmune and inflammatory phenotypes in *Trex1*$^{-/-}$ mice [18]. In addition, the accumulation of cytosolic dsDNA leads to fibroblast-like synoviocyte-mediated rheumatoid arthritis via the cGAS-STING pathway, and cGAS silencing inhibits the production of proinflammatory cytokines and relieves rheumatoid arthritis [19, 20]. Notably, cGAS has been reported to be involved in the pathogenesis of inflammatory bowel disease (IBD) [21–23]. The proinflammatory effect of cGAS is basically dependent on activation of the downstream STING-dependent inflammatory pathway. Abnormal cGAS-STING pathway activation induced by intestinal commensal bacteria can lead to intestinal inflammation, and silencing of cGAS alleviates the associated phenotype [23]. In addition, cGAS inhibition by the

[1]The First Affiliated Hospital of USTC, Division of Life Sciences and Medicine, University of Science and Technology of China, Hefei 230001, China; [2]Drug Discovery and Design Center, State Key Laboratory of Drug Research, Shanghai Institute of Materia Medica, Chinese Academy of Sciences, Shanghai 201203, China; [3]University of Chinese Academy of Sciences, Beijing 100049, China; [4]Shanghai Institute for Advanced Immunochemical Studies, and School of Life Science and Technology, Shanghai Tech University, Shanghai 200031, China and [5]School of Chinese Materia Medica, Nanjing University of Chinese Medicine, Nanjing 210023, China
Correspondence: Hua-liang Jiang (hljiang@simm.ac.cn) or Su-lin Zhang (slzhang@simm.ac.cn) or Ming-yue Zheng (myzheng@simm.ac.cn)
These authors contributed equally: Jia Song, Rui-rui Yang, Jie Chang, Ya-dan Liu

Received: 20 June 2022 Accepted: 19 September 2022
Published online: 13 October 2022

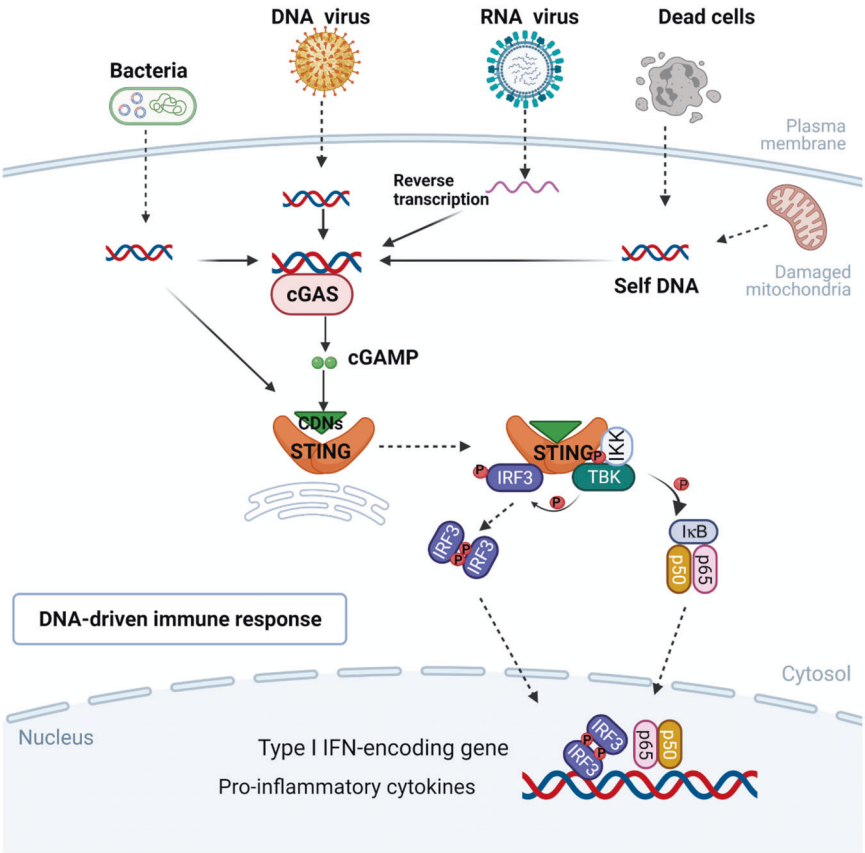

Fig. 1 cGAS-dependent innate immune signaling pathway.

specific inhibitor RU.521 alleviates intestinal colitis in GSDMD-deficient mice [22]. Therefore, inhibiting the cGAS-dependent innate immune signaling pathway is of vital importance for the treatment of autoimmune and inflammatory diseases, which has led to extensive efforts to examine potential cGAS inhibitors (Fig. 2).

Vincent et al. reported the first mouse cGAS (mcGAS) selective inhibitor RU.521, which binds to the catalytic pocket of mcGAS and selectively suppresses cGAS-mediated signaling in mouse macrophages [24]. RU.521 is currently the only reported mcGAS selective inhibitor with good cellular activity. PF-06928215, the first human cGAS (hcGAS) selective inhibitor, was reported to have high affinity for the catalytic site but exhibited no activity at the cellular level [25]. Compounds S2 and S3 are a novel class of selective hcGAS inhibitors and are also inactive at the cellular level, similar to PF-06928215 [26]. In addition, G150, CU32 and CU76 were described as new classes of small molecule hcGAS inhibitors with high binding capacity in vitro, as well as favorable cellular activity [27, 28]. Tan et al. reported that compound 25 was a structural modification of G140 and showed cellular activity with IC_{50} values of 1.38 μM and 11.4 μM against hcGAS and mcGAS, respectively [27, 29]. Although these compounds have demonstrated potency in vitro, in vivo validation in models is still insufficient. We need to develop more cGAS inhibitors with good in vivo activity to examine the role of cGAS in the pathogenesis of diseases. In this manuscript, we described a novel covalent cGAS inhibitor, 1-(1-phenyl-3,4-dihydro-1*H*-pyrrolo[1,2-a]pyrazin-2-yl) prop-2-yn-1-one (compound **3**), that was obtained by high-throughput screening and demonstrated better inhibitory activity and pathway selectivity than RU.521. More importantly, compound **3** exhibited promising therapeutic potential against DSS-induced colitis in a mouse model.

MATERIALS AND METHODS

Protein expression and purification

The nucleic acid sequences of mcGAS (full-length) and hcGAS (full-length) were inserted into the pSMART vector separately, and the proteins were tagged with His-sumo. The recombinant plasmid was transformed into the BL21 (DE3) strain (Shanghai Weidi Biotechnology Co., Ltd), which was cultured (37 °C) and induced with 0.3 mM IPTG overnight (16 °C). The cells were then collected and ultrasonically lysed. The cGAS protein was purified using a HiTrap 5 mL column. ULP-1 was used to split the His-sumo tag at 4 °C overnight. The protein was further purified using a heparin column and a Superdex75 10/300 GL column. The purified protein samples were concentrated and collected. The same protocol was used for the purification of mutant mcGAS (C419A).

PP_iase-coupled cGAS activity assay

The method of monitoring the enzymatic activity of mcGAS and hcGAS was developed by Zhao et al. with some modifications [26, 30, 31]. The screening reactions (40 μL) were performed using 384-well transparent polypropylene plates. The final concentrations of the compounds, cGAS, *Escherichia coli* pyrophosphatase (Sigma-Aldrich, I5907), HT-DNA (Sigma-Aldrich, D6898), ATP, and GTP were 200 μM, 200 nM, 50 nM, 5 μg/mL, 1 mM, and 300 μM, respectively. The liquid in the 384-well plate was centrifuged, followed by incubation for 90 min at room temperature (RT). The reaction was stopped by a quenching solution (40 μL, which contained 50 mM ethylenediaminetetraacetic acid, Sigma-Aldrich 03609) and malachite green solution (20 μL, Sigma-Aldrich 213020). Next, the mixture was incubated for 10 min (RT). The generation of cGAMP was normalized against the DMSO positive control (PC) and cGAS-Free negative control (NC) as follows: Inhibition % = 1 − (Abs sample − Abs mean NC)/(Abs PC-Abs NC).

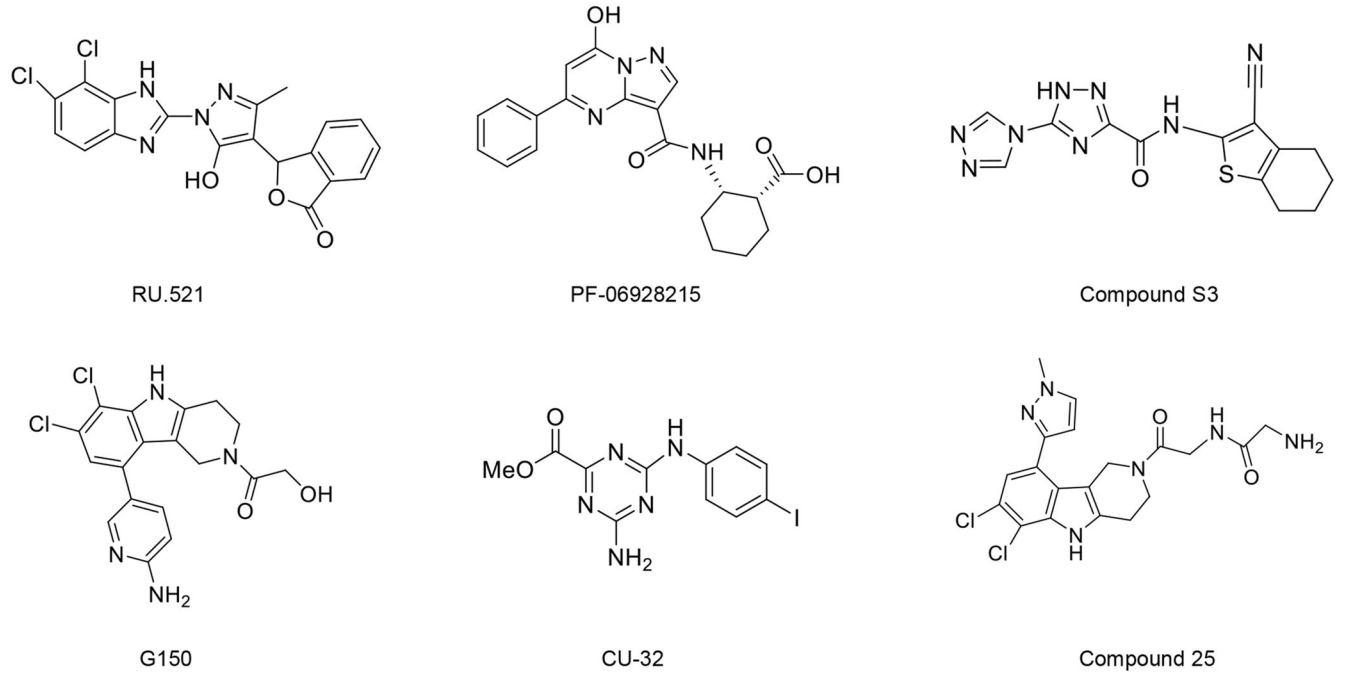

Fig. 2 Chemical structures of reported cGAS inhibitors.

Protein thermal shift assay

The thermostability of the mcGAS protein and hcGAS protein was tested using a CFX96^{TM} RealTime PCR Detection System (Bio-Rad). The compounds (12.5 μM) were mixed with mcGAS (1.25 μM) and 5× SYPRO orange (Invitrogen); 1-(1-phenyl-3,4-dihydro-1*H*-pyrrolo[1,2-a]pyrazin-2-yl)prop-2-yn-1-one (compound **3**) (25 μM) was mixed with hcGAS (1.25 μM) and 5× SYPRO orange. The signals of the reaction systems were continuously monitored and recorded from 25 °C to 90 °C for approximately 45 min.

dsDNA intercalation fluorescence polarization (FP) assay

The FP assay was used to test whether the compounds could intercalate DNA according to the reported protocol [24]. We used 384-solid bottom opaque plates (Corning, Cat No 3575) in this experiment. Each well contained 10 μL of 150 nM acridine orange, 10 μL of HT-DNA (37.5 μg/mL), and 10 μL of compounds. The DNA intercalator mitoxantrone served as a positive control. The reaction system was incubated for 30 min (RT), and then the fluorescence signals were measured on a Tecan Spark microplate reader (Tecan, Mannedorf, Switzerland).

dsDNA-cGAS interaction fluorescence polarization assay

We incubated 1 μL of compound **3** or unlabeled dsDNA with 20 μL of cGAS protein (2 μM) for 10 min (RT) and then added 20 μL of FAM-DNA (100 nM) and measured the fluorescence signals on a Tecan Spark microplate reader; DMSO or diluted buffer was used as a control. The dsDNA primers were as follows: Forward (FAM labeled): 5'-TACAGA^{FAM}TCTACTAGTGATCTATGACTGATCTGTACAT GATCTACA-3'; Forward (unlabeled): 5'-TACAGATCTACTAGTGATC TATGACTGATCTGTACATGATCTACA-3'; and Reverse: 5'-TGTAGAT CATGTACAGATCAGTCATAGATCACTAGTAGATCTGTA-3'. The DNA powder was dissolved in annealing buffer (50 mM Tris-HCl (pH 7.4), 1 mM DTT, 5% glycerol, 100 μg/mL BSA), and the forward and reverse primers were mixed at 1:1, annealed at 95 °C for 10 min, and slowly reduced to RT to form complementary double strands. The dilution buffer was 50 mM HEPES (pH 7.4).

Isothermal titration calorimetry (ITC)

The binding parameters of the compounds to mcGAS were measured with a MicroCal PEAQ-ITC calorimeter. The mcGAS protein was diluted to 50 μM. Then, 2 μL of the compound (200 μM) was added to the mcGAS protein every 180 s. The data were analyzed using MicroCal PEAQ-ITC software.

Nuclear magnetic resonance and mass spectrometry

A Bruker AVANCE III 600 MHz spectrometer was used to perform ligand-based NMR spectroscopy. The compounds were dissolved to 200 μM in the presence of 2.5, 5 or 10 μM mcGAS protein and 5% DMSO-d6.

To confirm the binding of mcGAS to compound **3**, 50 μM mcGAS (or mutation C419A) was incubated with 50 μM compound **3** at 4 °C for 8 h. The samples were analyzed by a QTOF mass spectrometer.

Covalent docking analysis

Molecular docking was conducted to analyze the possible binding mode of compound **3** and mcGAS. In short, mcGAS (PDB: 5XZG) was docked using Schrödinger (2018) in Covalent Docking Mode. We downloaded the mcGAS complex crystal structure (PDB number 5XZG) from the PDB protein crystal database (https://www.rcsb.org/structure/5XZG) and deleted the solvent molecule as a docking template. First, we used the Protein Preparation Wizard module in the Maestro software to prepare the receptor. Under the default parameters, the receptor was hydrogenated, the hydrogen bond grid was optimized, the residual matrix was protonated, and the receptor energy was minimized. Then, we used the LigPrep module to prepare the ligand, used Epik to calculate the possible ionic state of the ligand under the condition of pH = 7.4 ± 1.0, and generated a low-energy stereo conformation. After preparing the receptor and ligand, we selected residue Cys419 to be the reactive residue and defined the reaction type to be a Michael Addition. Finally, compound **3** was docked to the cGAS protein by using Covalent Docking Mode, and the top 5 poses were printed out.

Cell lines

Raw-Lucia ISG cells were purchased from InvivoGen (rawl-isg). Raw 264.7 cells were purchased from the Chinese Academy of Sciences Cell Bank (SCSP-5036). Mouse Raw macrophages were cultured in DMEM with 10% FBS and 1% penicillin-streptomycin at 37 °C in a

5% (*v*/*v*) CO_2 atmosphere. L929 cells were purchased from Procell (CL-0137) and cultured in MEM with 10% FBS and 1% penicillin-streptomycin at 37 °C in a 5% (*v*/*v*) CO_2 atmosphere. THP-1 cells were purchased from ATCC and cultured in RPMI- 1640 with 10% FBS and 1% penicillin-streptomycin at 37 °C in a 5% (*v*/*v*) CO_2 atmosphere.

Cellular luciferase assays

Raw-Lucia ISG cells (3000–5000/well) were plated on 96-well plates and cultured overnight, and then different concentrations of the compounds in fresh medium were added. After 12 h, the luciferase activity was measured using the QUANTI-Luc kit (InvivoGen rep-qlc1).

RT-qPCR

After Raw 264.7 cells, L929 cells and THP-1 cells were pretreated with the compounds for 2 h and transfected with Interferon Stimulatory DNA (ISD) or G3-ended Y-form Short DNA (G3-YSD) for 6 h, a Vazyme FastPure Cell/Tissue Total RNA Isolation Kit was used to extract total RNA. Next, gDNA wiper mix (Vazyme, R323-01-AB) was used to erase gDNA, and HiScript III qRT SuperMix (Vazyme, R323-01-AC) was used to synthesize cDNA. RT-qPCR was conducted using ChamQ SYBR qPCR Master Mix (Vazyme, Q331-AA) and primers in a CFX96 RealTime PCR Detection System. All the primer sequences used in the present work are shown below: mouse *Actb* forward (F): 5'-TGAGCTGCGTTTTACACCCT-3', mouse *Actb* reverse (R): 5'-GCCTTCACCGTTCCAGTTTT-3'; mouse *Ifnb1* F: 5'-GTCCTCAACTGCTCTCCACT-3', mouse *Ifnb1* R: 5'-CCTGCAACCAC CACTCATTC-3'; mouse *Cxcl10* F: 5'-ATCATCCCTGCGAGCCTATCCT-3', mouse *Cxcl10* R: 5'-GACCTTTTTTGGCTAAACGCTTTC-3'; mouse *Il6* F: 5'-ACAAGTCGGAGGCTTAATTACACAT-3', mouse *Il6* R: 5'-TT GCCATTGCACAACTCTTTTC-3'; mouse *Tnf* F: 5'-AGGCTGCCCCGAC-TACGT-3', mouse *Tnf* R: 5'-GACTTTCTCCTGGTATGAGATAGCAAA-3'; human *ACTB* F: 5'-CATGTACGTTGCTATCCAGGC-3', human *ACTB* R: 5'-CTCCTTAATGTCACGCACGAT-3'; human *IFNB1* F: 5'-CAGCATCTG CTGGTTGAAGA-3', human *IFNB1* R: 5'- CATTACCTGAAGGCCAAG GA-3'; and human *CXCL10* F: 5'-CCACGTGTTGAGATCATTGCT-3', human *CXCL10* R: 5'-TGCATCGATTTTGCTCCCCT-3'.

Transcriptomic analysis

Raw 264.7 cells were pretreated with compound **3** for 2 h, followed by transfection with ISD for an additional 6 h. Total RNA was extracted for RNA sequencing by Majorbio (www.majorbio.com). We processed the RNA sequencing data using the Majorbio Cloud Platform.

Cell Titer Glo viability assay

We plated Raw 264.7 cells and L929 cells into 96-well plates separately and added different doses of compound **3** the next day. After 8 h, cell viability was measured by Cell Titer Glo (CTG; Promega, G7570) according to the manufacturer's protocol.

Western blotting

We plated Raw 264.7 cells into 6-well plates, followed by pretreatment with different doses of the compounds for 2 h. Then, the cells were transfected with ISD for an additional 6 h. After that, total proteins were isolated from Raw 264.7 cells using RIPA lysis buffer (Beyotime Biotechnology, P0013B) containing phosphatase inhibitor (Bimake, 510031) and protease inhibitor (Bimake, B14012). The cell lysates were centrifuged, and the total protein in the supernatant was determined by a BCA kit. Total proteins (25 μg) were loaded onto polyacrylamide gels and transferred onto nitrocellulose membranes, which were blocked with milk (5%, BD, 232100), followed by incubation using the different primary antibodies at 4 °C (overnight) and HRP-conjugated secondary antibody (Promega, W4028) (RT) (1.5 h). The membranes were incubated with the ECL kit (Meilun, MA0186). We obtained the following antibodies from Cell Signaling Technology: anti-p-STING (72971), anti-STING (13647), anti-p-TBK1 (5483), anti-TBK1 (3504), anti-p-IRF3 (29047), anti-IRF3 (4302), and anti-tubulin (15115). Finally, the signals were detected and analyzed using GeneGnome XRQ NPC (Shanghai, China).

Determination of intracellular cGAMP level

Raw 264.7 cells were pretreated with compound **3** for 2 h, followed by transfection with ISD for an additional 6 h. Then, we used a 2′,3′-Cyclic GAMP Enzyme Immunoassay Kit (Arbor Assays, K067-H1) to determine the intracellular cGAMP level according to the manufacturer's protocol.

Animal experiments: Colitis Model

All procedures performed on animals were in accordance with regulations and established guidelines and were reviewed and approved by the Institutional Animal Care and Use Committee of Shanghai Institute of Materia Medica, Chinese Academy of Sciences. C57BL/6 J mice were obtained from Sippr-BK Laboratory Animal Co., Ltd. (Shanghai, China). C57BL/6 J mice aged 6 to 8 weeks were used in our studies. Drinking water containing 3% (*w*/*v*) DSS (MP Biomedicals) was given to mice every other day for 9 days to establish an acute colitis model [32]. During the last two days of the experiment, the feeding water was replaced with normal water for sampling. Compound **3** was injected intraperitoneally at a dose of 20 mg/kg once daily during DSS-induced colitis. On Day 11, the intestinal tissues and serum were collected for analysis.

Cytokine measurement

IL-6 and TNF levels in mouse serum were detected by ELISA kits (Absin Bioscience Inc.) according to the manufacturer's instructions. In summary, extracted mouse serum (20 μL) was added into the corresponding wells, followed by incubation (RT) and washing with detergent. After the liquid was patted dry, 100 μL of detection antibody was added to each well and incubated the plate for 2 h (RT). Each plate was rinsed repeatedly. Streptavidin (100 μL) was added to each well and incubated for 20 min (RT). After the plates were washed, streptavidin-HRP (100 μL) was added to each well and incubated for 20 min (RT). Finally, stop solution (50 μL) was added to each well, and the OD values were detected at 450 nm.

H&E staining

Colorectal samples were collected from the mice at the end of the experiment, and the lengths were recorded. A section of the colorectum (approximately 5 cm) was cut and stained, followed by analysis by Servicebio (https://www.servicebio.cn).

Statistical analysis

GraphPad Prism 8.0 was used for statistical analyses. All numerical results are displayed as the mean ± SD. Differences in quantitative data between groups were calculated using a 2-tailed unpaired *t*-test. The significance level was set as follows: ns, no statistical difference, $P > 0.05$; $^{*}P < 0.05$; $^{**}P < 0.01$; $^{***}P < 0.001$.

RESULTS

Discovery of cGAS inhibitors via PP_iase-coupled activity assay

The enzymatic activity of cGAS was determined with a PP_iase coupling assay as reported by Zhao et al. with some modifications [26]. As shown in Fig. 3a, cGAS uses GTP and ATP to produce cGAMP and two inorganic pyrophosphates (PP_i), which are rapidly and irreversibly hydrolyzed by inorganic pyrophosphatase to inorganic phosphate (P_i). The enzymatic activity of cGAS is indicated by the amount of P_i in the reaction system, which can be detected through conventional phosphomolybdate-malachite green absorbance methodology. We first tested the inhibitory

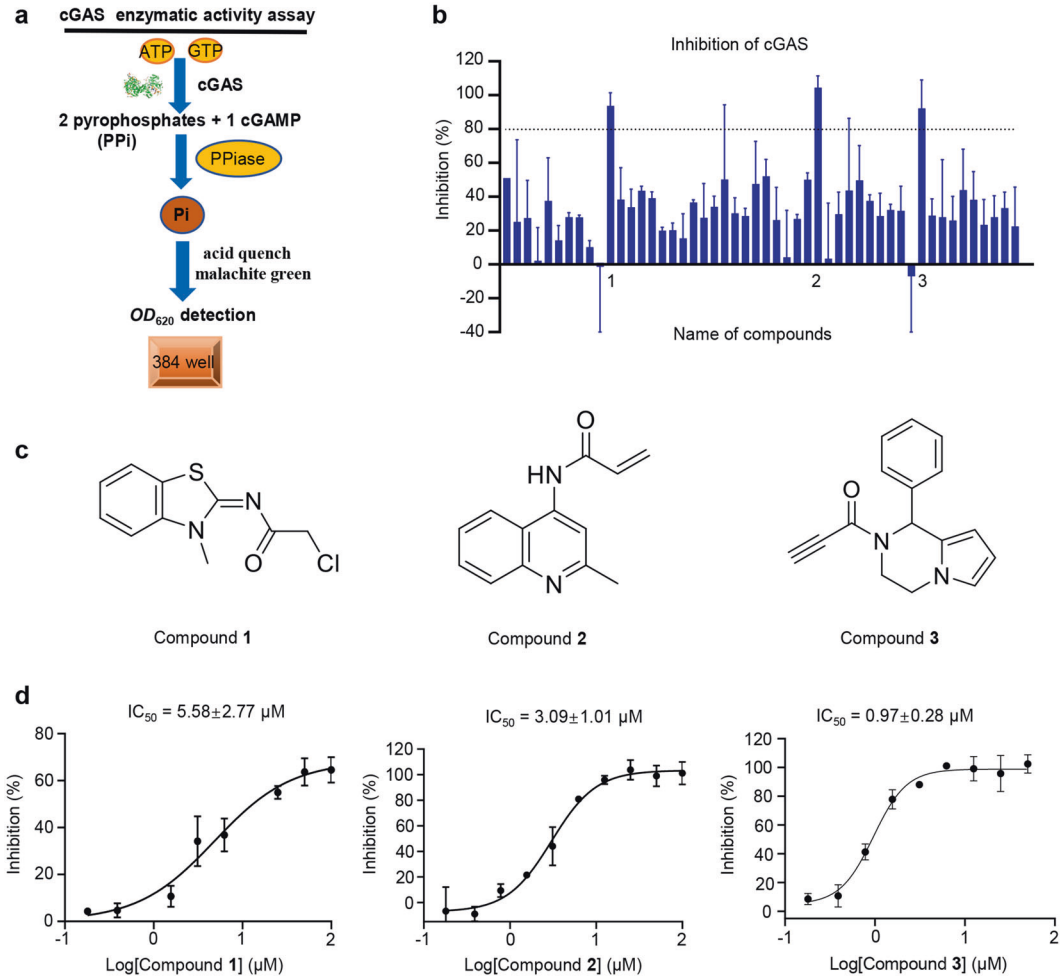

Fig. 3 Discovery of cGAS inhibitors. a Screening workflow of the PP$_i$ase-coupled assay. **b** The inhibition ratio of 50 selected compounds. **c** Chemical structures of compounds **1-3**. **d** The inhibitory effect of compounds **1-3** against mcGAS enzymatic activity was measured by the PP$_i$ase-coupled assay. The data are shown as the mean ± SD of at least three independent experiments.

effect of the reported mcGAS inhibitor RU.521 on purified recombinant mcGAS protein. The results showed that RU.521 could inhibit the catalytic activity of mcGAS with an IC_{50} of 0.74 ± 0.12 μM (Supplementary Fig. S1a), which was similar to previously reported results [24], suggesting that this PP$_i$ase-coupled assay could be used to screen cGAS inhibitors. Using this high-throughput PP$_i$ase-coupled activity assay, a total of 25,000 compounds from our in-house library were used for screening. Then, based on the enzymatic activity data of the preliminary screening, 50 compounds with better inhibitory effects and physicochemical properties were selected for purchase and retesting. Among the 50 candidates, compounds **1**, **2** and **3** (Fig. 3b, c) displayed an almost 100% inhibition ratio at a concentration of 50 μM. Therefore, compounds **1-3** were chosen for further research. Compounds **1-3** inhibited cGAS enzymatic activity with IC_{50} values of 5.58 μM, 3.09 μM and 0.97 μM, respectively (Fig. 3d).

Compounds **1-3** directly bind to cGAS in vitro

To investigate whether compounds **1-3** directly bind to cGAS in vitro, the protein thermal shift assay was first performed. The results showed that compounds **1-3** enhanced the thermal stability of mcGAS and increased the Tm values of cGAS by 3.5 °C, 5.5 °C and 4 °C, respectively (Fig. 4a). We further tested the direct binding of compounds **1-3** with cGAS using nuclear magnetic resonance (NMR). Only compound **3** showed signal attenuation in the T1ρ NMR spectra, as well as positive saturation transfer difference (STD) signals in the STD spectrum, suggesting that compound **3** directly binds to cGAS (Fig. 4b). Considering compound **3** with a covalent warhead, we performed a mass spectrometry (MS) to analyze whether compound **3** could covalently bind to the cGAS protein. As expected, compound **3** covalently bound to cGAS (Fig. 4c). Next, we attempted to illustrate the potential binding mode between compound **3** and cGAS (PDB: 5XZG) by covalent docking-based molecular simulation. As shown in Fig. 4d, the docking pose indicates that compound **3** can form a covalent bond with Cys419 in the binding pocket. Additionally, compound **3** forms a π-cation interaction with Lys350, and the benzene ring of compound **3** extends into the hydrophobic pocket of cGAS, which stabilizes the interaction between compound **3** and cGAS. In short, this docking pose explains the activity of compound **3** and is consistent with the covalent docking score of −3.955. The MS results also confirmed that Cys419 of cGAS was modified by compound **3** (Fig. 4c). The K_D value of the interaction between cGAS and compound **3** was 1.21 μM, as determined by isothermal titration calorimetry (ITC) assay (Fig. 4e). Since blocking the interaction between dsDNA and cGAS protein can also affect the catalytic activity of cGAS, we investigated whether compounds **1-3** could intercalate into DNA by the acridine orange-based fluorescence polarization (FP) method. The mP values showed that compounds **1-3** do not intercalate into dsDNA, suggesting that the inhibition of cGAS enzymatic activity by compounds **1-3** is not due to intercalation

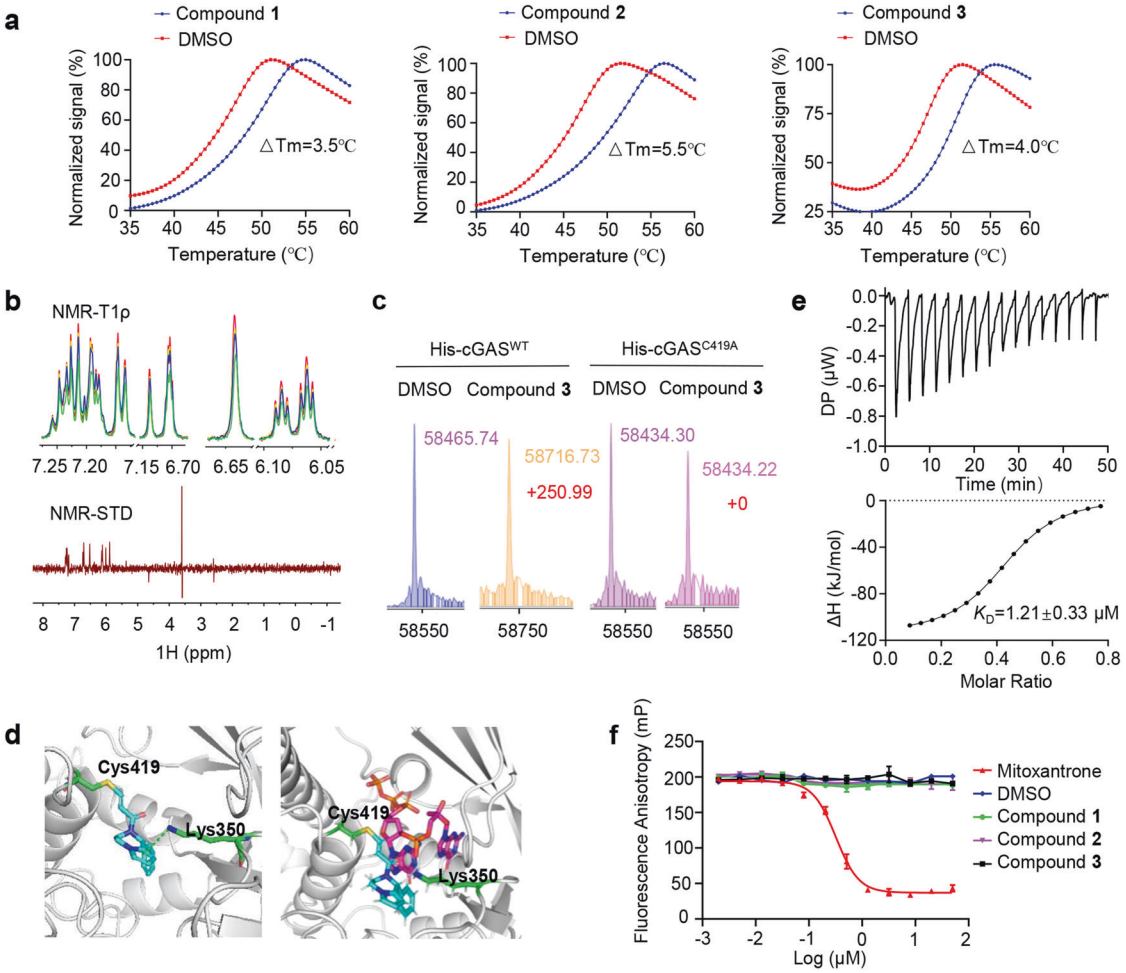

Fig. 4 Compounds 1-3 directly bind to mcGAS. a The melting curve of the mcGAS protein (1.25 μM) treated with compounds **1-3** (12.5 μM). **b** NMR measurement of the direct binding of compound **3** with mcGAS. T1ρ NMR spectra for compound **3** (red) and compound **3** in the presence of mcGAS at 5 μM (green), 2.5 μM (blue), and 1.25 μM (yellow). The STD spectrum for compound **3** in the presence of mcGAS (2.5 μM). **c** QTOF mass spectra of wild-type mcGAS and C419A mutant mcGAS. mcGAS was incubated with compound **3** or DMSO at 4 °C for 8 h. The QTOF mass spectra results showing the molecular weight of modified mcGAS (yellow and pink). **d** Left: Binding mode prediction of mcGAS with compound **3**; right: binding mode simulation of mcGAS with compound **3** and the intermediate product 5′-pppdG(2′,5′)pdG. Compound **3** is shown as blue sticks, and 5′-pppdG(2′,5′)pdG is shown as purple sticks. **e** ITC-binding curves for compound **3** titrated with mcGAS. The top graph represents the raw ITC thermograms, and the bottom graph represents the fitted binding isotherms. **f** The ability of compounds **1-3** to intercalate into dsDNA was tested by FP assays. Mitoxantrone, a known DNA intercalator, was a positive control. The data are shown as the mean ± SD of at least three independent experiments.

into dsDNA (Fig. 4f). In addition, to clarify how compound **3** affects cGAS enzymatic activity, we next examined whether compound **3** blocks the binding of substrates to the catalytic pocket of cGAS or allosterically influences the binding of cGAS to dsDNA. First, we established a fluorescence polarization assay using FAM-labeled dsDNA and cGAS protein, which can directly detect the interaction between dsDNA and cGAS protein. The results showed that compound **3** did not influence the binding of cGAS to dsDNA (Supplementary Fig. S1b). Moreover, molecular docking simulation of cGAS with compound **3** showed that compound **3** binding to cGAS hindered the binding of the substrate (Fig. 4d). Overall, we demonstrated that compound **3** could covalently bind to Cys419 of mcGAS and block the binding of substrates to the catalytic pocket of mcGAS rather than allosterically influencing the binding of cGAS to dsDNA.

Compound **3** selectively inhibits cGAS-mediated signaling

To evaluate the capability of compounds **1-3** to inhibit cGAS-mediated signaling at the cellular level, we examined the efficacy of compounds **1-3** on suppressing ISD-dependent activation of cGAS in Raw-Lucia ISG cells (InvivoGen). Compounds **1-3** exhibited obvious inhibition with IC_{50} values ranging from 0.51 μM to 2.71 μM (Fig. 5a, Supplementary Fig. S2a, b). Compound **3** was the best at inhibiting ISD-stimulated cGAS activation, with an IC_{50} of 0.51 μM, which was superior to that of RU.521 (Fig. 5a, Supplementary Fig. S2c). In addition, compounds **1-3** could significantly suppress the transcription of *Ifnb1*, *Cxcl10* and *Il6* triggered by ISD stimulation (Fig. 5b, Supplementary Fig. S3a, b). To evaluate whether compounds **1-3** could affect other innate immune signaling pathways other than ISD activation, Raw 264.7 cells were stimulated with other immunostimulants, including poly(I:C) (RIG-I/MDA5 agonist), IFN-β (JAK/STAT pathway agonist), Pam3CSK4 (TLR1/2 agonist), cGAMP and ADU-S100 (STING agonist). Except for its ability to suppress ISD stimuli, compound **3** was unable to inhibit any other immunogenic stimuli (Fig. 5c-f, Supplementary Fig. S3c, d). In contrast, compounds **1-2** could significantly inhibit poly(I:C) or cGAMP or ADU-S100 stimulation (Fig. 5c-f, Supplementary Fig. S3c, d). We found that RU.521 could inhibit *Cxcl10* transcription in Raw 264.7 cells after transfection with poly(I:C)

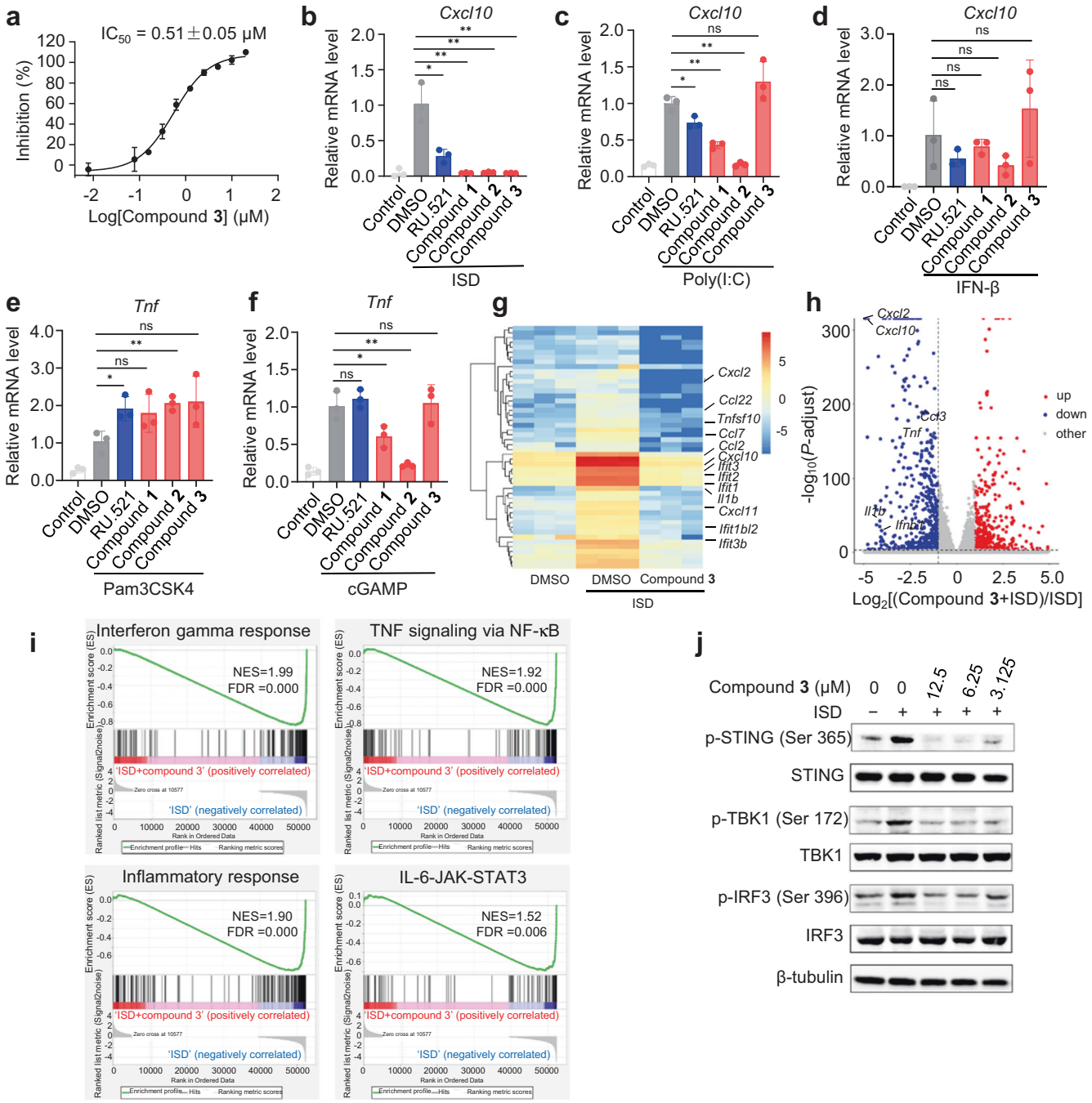

Fig. 5 Compound 3 selectively inhibits cGAS-mediated signaling. a The inhibitory effect of compound **3** against the IFN response induced by ISD in Raw-Lucia ISG cells. **b**–**f** Raw 264.7 cells were incubated with compounds **1-3** or RU.521 at a dose of 10 μM for 2 h. Then, for cGAS-STING signaling, the cells were stimulated with ISD (1 μg/mL) or cGAMP (20 μM) for 6 h. For other signaling pathways, the cells were stimulated with the following immunostimulants: 1.5 μg/mL poly(I:C), 2.5×10^5 U/mL recombinant murine interferon-β (IFN-β), and 1 μg/mL Pam3CSK4 for 18 h. All cells were harvested for RT-qPCR analysis. **g** Heatmap of RNA sequencing data for Raw 264.7 cells treated with DMSO or ISD with or without compound **3**. The 50 genes with the highest inhibition rates are shown in cells treated with compound **3**. **h** Volcano plot of RNA sequencing data for dsDNA-stimulated Raw 264.7 cells in the presence or absence of compound **3**. The differentially expressed genes were defined as *P* adjusted <0.01 and $\log_2$ (fold change) > 1 or <−1. **i** Downregulated GSEA signatures in ISD-stimulated Raw 264.7 cells after treatment with compound **3**. NES, normalized enrichment score; FDR, *P* adjusted value. **j** Raw 264.7 cells were incubated with DMSO or compound **3** for 2 h and transfected with ISD for an additional 6 h, and the indicated proteins were then examined. The data in figures (**b**–**f**) are shown as the mean ± SD of at least three independent experiments; a two-tailed unpaired *t*-test was used to analyze significant differences between groups. ns, no statistical difference; **P* < 0.05; ***P* < 0.01.

(Fig. 5c), suggesting that RU.521 may have cross-inhibitory activity against RIG-I/MDA5. Overall, these results demonstrate that compound **3** has better activity and target specificity at the cellular level than RU.521. In addition, compound **3** also suppressed the transcription of *Ifnb1* and *Cxcl10* triggered by ISD stimulation in L929 cells (Supplementary Fig. S4a). We also detected the level of intracellular cGAMP induced by the transfection of ISD, and the results showed that compound **3**

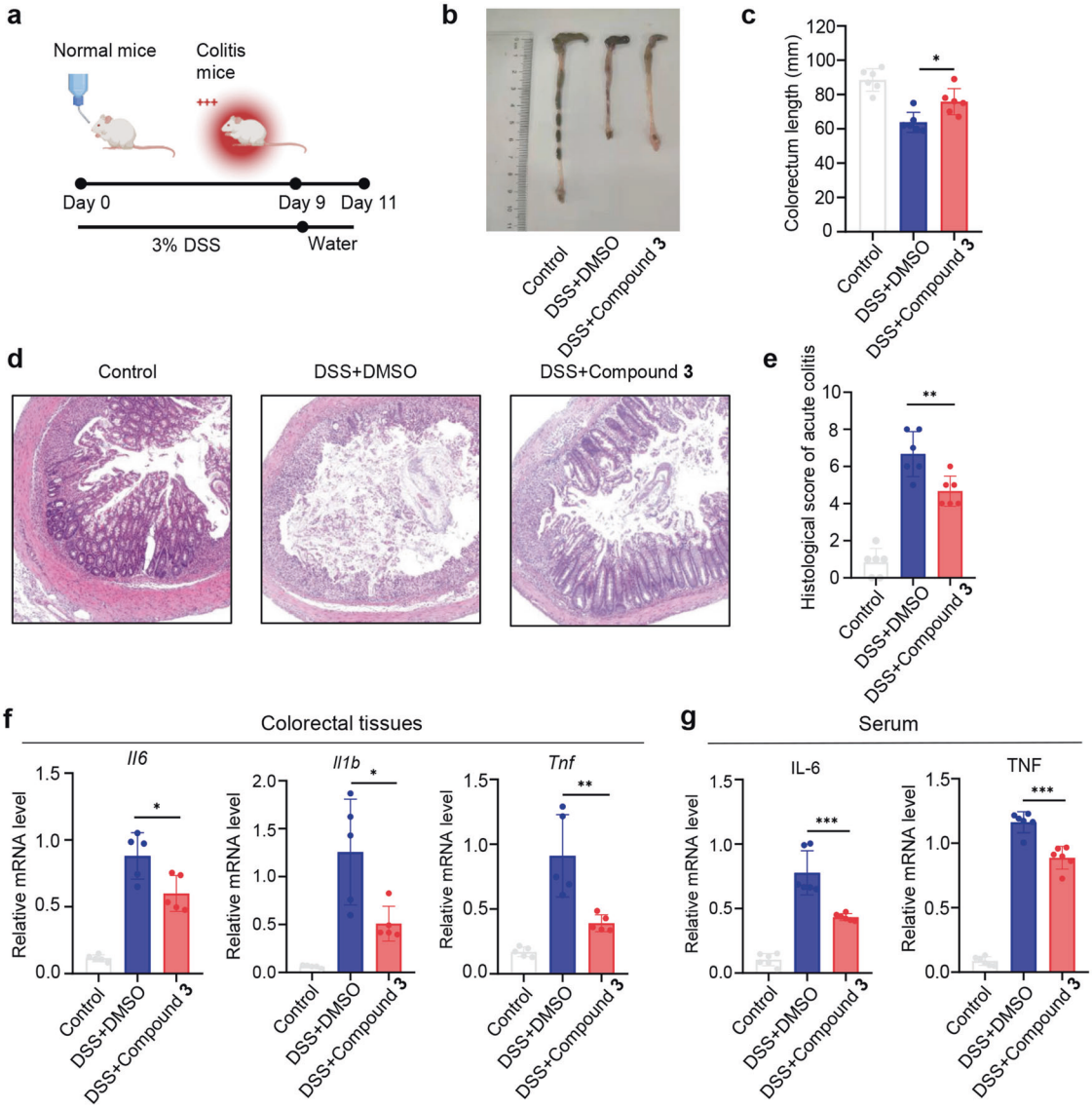

Fig. 6 Compound 3 ameliorates DSS-induced colitis in mice. a Process of establishing the colitis mouse model. C57BL/6 J mice were fed 3% DSS (aqueous solution) for 9 days and then fed water for 2 days. Compound **3** was injected intraperitoneally at a dose of 20 mg·kg^{-1}·d^{-1} ($n = 6$). **b**–**c** After the experiment, the mice were euthanized, and the length of the colon was measured ($n = 6$). **d**–**e** Representative colonic histological images and colonic inflammation scores ($n = 6$). **f** The mRNA levels of *Il6*, *Il1b* and *Tnf* in the colonic tissues of C57BL/6 J mice ($n = 5$). **g** The concentrations of IL-6 and TNF in the serum of C57BL/6 J mice were measured using ELISA ($n = 6$). The data in figures (**c**, **e**–**g**) are shown as the mean ± SD, and a two-tailed unpaired *t*-test was used to analyze significant differences between groups. *$P < 0.05$; **$P < 0.01$; ***$P < 0.001$.

dose-dependently inhibited the production of cGAMP (Supplementary Fig. S4b). The cytotoxicity experiments on Raw 264.7 and L929 cells showed that compound **3** did not affect cell viability within the experimental concentration range, suggesting that the inhibitory effect of compound **3** on cGAS activation was not caused by cytotoxicity (Supplementary Fig. S4c, d). To further confirm the cellular activity of compound **3**, we next performed global transcriptomic analysis of ISD-stimulated Raw 264.7 cells in the presence or absence of compound **3**. The results revealed that compound **3** could downregulate 90% of ISD-stimulating genes, including ISGs and proinflammatory cytokines (*Cxcl2*, *Cxcl10* and *Il1b*) (Fig. 5g-h). Consistently, differential gene set enrichment analysis (GSEA) showed that the 'interferon gamma response', 'TNF signaling via NF-κB', 'inflammatory response', and 'IL-6-JAK-STAT3' signatures were enriched (Fig. 5i). In addition, immunoblotting was conducted to evaluate the effect of compound **3** on the cGAS-STING signaling pathway in Raw 264.7 cells. The results showed that compound **3** markedly reduced the phosphorylation levels of STING and its downstream proteins TBK1 and IRF3, which were induced by ISD (Fig. 5j). Collectively, these results strongly suggest that compound **3** is a potent and selective inhibitor of mcGAS.

Compound **3** alleviates DSS-induced colitis in mice

As previously reported, cGAS is involved in the pathogenesis of IBD. Wang et al. reported that cGAS is a potential biomarker of IBD and that cGAS knockout in mice alleviated the inflammatory response [21]. Ahn et al. reported that symbiotic bacteria induce the production of inflammatory cytokines in mononuclear phagocytes by activating the cGAS-STING pathway. Silencing cGAS can significantly reduce intestinal inflammation [23]. Moreover, in GSDMD-deficient mice, the intraperitoneal injection of cGAS inhibitor RU.521 can alleviate intestinal colitis [22].

Therefore, we further investigated whether compound **3** could be used to treat DSS-induced IBD in mice (Fig. 6a). Colon length reduction is a hallmark of the DSS-induced IBD mouse model, and treatment with compound **3** dramatically improved the reduction in colon length (Fig. 6b, c). Histological staining showed that DSS caused inflammatory cell infiltration, epithelial cell injury and crypt swelling and destruction in the colon sections of mice, and these features were improved after treatment with compound **3** (Fig. 6d); moreover, the histological score of acute colitis was obviously reduced (Fig. 6e). Furthermore, the mRNA levels of *Il6, Il1b* and *Tnf* in colon sections of DSS model mice were examined, and compound **3** significantly reduced the expression levels of these cytokines (Fig. 6f). Similarly, the levels of IL-6 and TNF in the serum of DSS model mice were significantly increased but were decreased after compound **3** treatment (Fig. 6g). In summary, our data demonstrate that compound **3** significantly alleviates DSS-induced colitis in mice.

CONCLUSION AND DISCUSSION

Herein, we described the discovery and validation of the potent and selective mcGAS inhibitor compound **3**. Protein thermal shift, nuclear magnetic resonance and isothermal titration calorimetry assays confirmed that compound **3** could directly bind to the mcGAS protein. MS and subsequent mutant analysis revealed that compound **3** could covalently bind to Cys419 of cGAS. Compound **3** did not intercalate into dsDNA or interfere with the interaction between cGAS and dsDNA, which also suggests that its inhibition of cGAS catalytic activity was due to direct binding to the cGAS protein and blocking the binding of substrates to the catalytic pocket of cGAS. Although the mechanisms of dsDNA sensing and cGAMP production are conserved between human and mouse cGAS, human and mouse cGAS only share 60% amino acid identity, suggesting that drug screening to inhibit both human and mouse cGAS with high potency and cellular activity may be difficult. In fact, this is exactly the case, and the reported cGAS inhibitors are almost all selective inhibitors of mouse or human cGAS. Our data indicate that compound **3** has good inhibitory activity against mouse cGAS but relatively weaker activity against human cGAS (Supplementary Fig. S5a–c), suggesting that compound **3** is a selective mouse cGAS inhibitor. Vincent et al. reported RU.521, the first selective mouse cGAS inhibitor that binds to the substrate binding pocket of mouse cGAS and selectively suppresses cGAS-mediated signaling in mouse macrophages [24]. RU.521 is currently the only selective mouse cGAS inhibitor with good cellular activity that has been reported. The inhibitory effect of compound **3** on mouse cGAS was similar to that of RU.521. Compound **3** inhibited ISD-stimulated cGAS activation with an IC_{50} of 0.51 ± 0.05 μM, which was superior to that of RU.521 (2.41 ± 0.87 μM) in our study. Most of the reported cGAS inhibitors, including RU.521, act on the substrate binding pocket of cGAS, while compound **3** covalently binds to Cys419 around the pocket and has better pathway selectivity at the cellular level than RU.521, which provides inspiration for the development of novel and highly selective cGAS inhibitors. Cys419 is not conserved in murine and human cGAS proteins (Supplementary Fig. S5d), which explains the weak activity of compound **3** against human cGAS. Although a number of mouse and human cGAS inhibitors have demonstrated potency in vitro [25–28], in vivo validation in models is still insufficient. In our study, compound **3** alleviated DSS-induced colitis in mice, indicating that compound **3** has the potential to be further developed for inflammatory disease therapies.

ACKNOWLEDGEMENTS

We gratefully acknowledge financial support from the National Natural Science Foundation of China (T2225002 and 82273855 to MYZ; 81903639 to SLZ), Lingang Laboratory (LG202102-01-02 to MYZ; LG-QS-202204-01 to SLZ), the Shanghai Municipal Science and Technology Major Project, and the Natural Science Foundation of Shanghai (22ZR1474300 to SLZ).

AUTHOR CONTRIBUTIONS

Conception of the hypothesis: MYZ and SLZ; Study supervision: MYZ, SLZ, HLJ, KXC and XML; Development of methodology: JS, RRY and CHL. Acquisition of data: JS, RRY, JC, YDL, CHL, LFC, HG, YHZ, ZSF, and JYZ. Analysis and interpretation of data: JS, RRY, JC, YDL, CHL, LFC, HG, YHZ, ZSF, JYZ, GZZ, and KKZ. Writing and review of the manuscript: SLZ, JS, RRY, JC and YDL. All authors discussed the study.

ADDITIONAL INFORMATION

Supplementary information The online version contains supplementary material available at https://doi.org/10.1038/s41401-022-01002-5.

Competing interests: The authors declare no competing interests.

REFERENCES

1. Hu MM, Shu HB. Cytoplasmic mechanisms of recognition and defense of microbial nucleic acids. Annu Rev Cell Dev Biol. 2018;34:357–79.
2. Collins Angela C, Cai H, Li T, Franco Luis H, Li XD, Nair Vidhya R, et al. Cyclic GMP-AMP synthase is an innate immune DNA sensor for mycobacterium tuberculosis. Cell Host Microbe. 2015;17:820–8.
3. Zhang X, Wu J, Du F, Xu H, Sun L, Chen Z, et al. The cytosolic DNA sensor cGAS forms an oligomeric complex with DNA and undergoes switch-like conformational changes in the activation loop. Cell Rep. 2014;6:421–30.
4. Wu J, Sun L, Chen X, Du F, Shi H, Chen C, et al. Cyclic GMP-AMP is an endogenous second messenger in innate immune signaling by cytosolic DNA. Science. 2013;339:826–30.
5. Sun L, Wu J, Du F, Chen X, Chen ZJ. Cyclic GMP-AMP synthase is a cytosolic DNA sensor that activates the type I interferon pathway. Science. 2013;339:786–91.
6. Ablasser A, Goldeck M, Cavlar T, Deimling T, Witte G, Rohl I, et al. cGAS produces a 2′-5′-linked cyclic dinucleotide second messenger that activates STING. Nature. 2013;498:380–4.
7. Burdette DL, Monroe KM, Sotelo-Troha K, Iwig JS, Eckert B, Hyodo M, et al. STING is a direct innate immune sensor of cyclic di-GMP. Nature. 2011;478:515–8.
8. Jin L, Hill KK, Filak H, Mogan J, Knowles H, Zhang B, et al. MPYS is required for IFN response factor 3 activation and type I IFN production in the response of cultured phagocytes to bacterial second messengers cyclic-di-AMP and cyclic-di-GMP. J Immunol. 2011;187:2595–601.
9. Zhong B, Yang Y, Li S, Wang YY, Li Y, Diao F, et al. The adaptor protein MITA links virus-sensing receptors to IRF3 transcription factor activation. Immunity. 2008;29:538–50.
10. Balka KR, Louis C, Saunders TL, Smith AM, Calleja DJ, D'Silva DB, et al. TBK1 and IKKepsilon act redundantly to mediate STING-induced NF-kappaB responses in myeloid cells. Cell Rep. 2020;31:107492.
11. Tanaka Y, Chen ZJ. STING specifies IRF3 phosphorylation by TBK1 in the cytosolic DNA signaling pathway. Sci Signal. 2012;5:ra20.
12. Civril F, Deimling T, de Oliveira Mann CC, Ablasser A, Moldt M, Witte G, et al. Structural mechanism of cytosolic DNA sensing by cGAS. Nature. 2013;498:332–7.
13. Chen Q, Sun L, Chen ZJ. Regulation and function of the cGAS-STING pathway of cytosolic DNA sensing. Nat Immunol. 2016;17:1142–9.
14. Ablasser A, Chen ZJ. cGAS in action: expanding roles in immunity and inflammation. Science. 2019;363:eaat8657.
15. Xiao N, Wei J, Xu S, Du H, Huang M, Zhang S, et al. cGAS activation causes lupus-like autoimmune disorders in a TREX1 mutant mouse model. J Autoimmun. 2019;100:84–94.
16. Ablasser A, Hemmerling I, Schmid-Burgk JL, Behrendt R, Roers A, Hornung V. TREX1 deficiency triggers cell-autonomous immunity in a cGAS-dependent manner. J Immunol. 2014;192:5993–7.
17. Gray EE, Treuting PM, Woodward JJ, Stetson DB. Cutting Edge: cGAS is required for lethal autoimmune disease in the Trex1-deficient mouse model of Aicardi-Goutieres syndrome. J Immunol. 2015;195:1939–43.
18. Gao D, Li T, Li XD, Chen X, Li QZ, Wight-Carter M, et al. Activation of cyclic GMP-AMP synthase by self-DNA causes autoimmune diseases. Proc Natl Acad Sci USA. 2015;112:E5699–705.
19. Wang Y, Su GH, Zhang F, Chu JX, Wang YS. Cyclic GMP-AMP synthase is required for cell proliferation and inflammatory responses in rheumatoid arthritis synoviocytes. Mediators Inflamm. 2015;2015:192329.
20. Wang J, Li R, Lin H, Qiu Q, Lao M, Zeng S, et al. Accumulation of cytosolic dsDNA contributes to fibroblast-like synoviocytes-mediated rheumatoid arthritis synovial inflammation. Int Immunopharmacol. 2019;76:105791.

21. Wang Z, Guo K, Gao P, Pu Q, Lin P, Qin S, et al. Microbial and genetic-based framework identifies drug targets in inflammatory bowel disease. Theranostics. 2021;11:7491–506.
22. Ma C, Yang D, Wang B, Wu C, Wu Y, Li S, et al. Gasdermin D in macrophages restrains colitis by controlling cGAS-mediated inflammation. Sci Adv. 2020;6:eaaz6717.
23. Ahn J, Son S, Oliveira SC, Barber GN. STING-dependent signaling underlies IL-10 controlled inflammatory colitis. Cell Rep. 2017;21:3873–84.
24. Vincent J, Adura C, Gao P, Luz A, Lama L, Asano Y, et al. Small molecule inhibition of cGAS reduces interferon expression in primary macrophages from autoimmune mice. Nat Commun. 2017;8:750.
25. Hall J, Brault A, Vincent F, Weng S, Wang H, Dumlao D, et al. Discovery of PF-06928215 as a high affinity inhibitor of cGAS enabled by a novel fluorescence polarization assay. PLoS One. 2017;12:e0184843.
26. Zhao W, Xiong M, Yuan X, Li M, Sun H, Xu Y. In silico screening-based discovery of novel inhibitors of human cyclic GMP-AMP synthase: a cross-validation study of molecular docking and experimental testing. J Chem Inf Model. 2020;60:3265–76.
27. Lama L, Adura C, Xie W, Tomita D, Kamei T, Kuryavyi V, et al. Development of human cGAS-specific small-molecule inhibitors for repression of dsDNA-triggered interferon expression. Nat Commun. 2019;10:2261.
28. Padilla-Salinas R, Sun L, Anderson R, Yang X, Zhang S, Chen ZJ, et al. Discovery of small-molecule cyclic GMP-AMP synthase inhibitors. J Org Chem. 2020;85:1579–600.
29. Tan J, Wu B, Chen T, Fan C, Zhao J, Xiong C, et al. Synthesis and pharmacological evaluation of tetrahydro-gamma-carboline derivatives as potent anti-inflammatory agents targeting cyclic GMP-AMP synthase. J Med Chem. 2021;64:7667–90.
30. Hooy RM, Sohn J. The allosteric activation of cGAS underpins its dynamic signaling landscape. Elife. 2018;7:e39984.
31. Seamon KJ, Stivers JT. A high-throughput enzyme-coupled assay for SAMHD1 dNTPase. J Biomol Screen. 2015;20:801–9.
32. Zhao F, Zheng T, Gong W, Wu J, Xie H, Li W, et al. Extracellular vesicles package dsDNA to aggravate Crohn's disease by activating the STING pathway. Cell Death Dis. 2021;12:815.